JACS
JOURNAL OF THE AMERICAN CHEMICAL SOCIETY

Communication

A Stable Blue Photosensitizer for Color Palette of Dye-Sensitized Solar Cells Reaching 12.6% Efficiency

Yameng Ren, Danyang Sun, Yiming## Cao#, Hoi Nok Tsao, Yi Yuan, Shaik M. Zakeeruddin, Peng Wang, and Michael Grätzel

J. Am. Chem. Soc., **Just Accepted Manuscript** • DOI: 10.1021/jacs.7b12348 • Publication Date (Web): 11 Jan 2018

Just Accepted

ACS Publications

Journal of the American Chemical Society is published by the American Chemical Society. 1155 Sixteenth Street N.W., Washington, DC 20036

A Stable Blue Photosensitizer for Color Palette of Dye-Sensitized Solar Cells Reaching 12.6% Efficiency

Yameng Ren,[†,‡] Danyang Sun,[†] Yiming Cao,[‖] Hoi Nok Tsao,[‖] Yi Yuan,[†] Shaik M. Zakeeruddin,[‖] Peng Wang,*[†] and Michael Grätzel*[‖]

[†]Center for Chemistry of Novel & High-Performance Materials, Department of Chemistry, Zhejiang University, 310028 Hangzhou, China

[‡]Changchun Institute of Applied Chemistry, Chinese Academy of Sciences, 130022 Changchun, China

[‖]Laboratory of Photonics and Interfaces, Institute of Chemical Sciences & Engineering, École Polytechnique Fédérale de Lausanne, CH-1015 Lausanne, Switzerland

Supporting Information Placeholder

ABSTRACT: We report a blue dye, coded as R6, which features a polycyclic aromatic hydrocarbon 9,19-dihydrobenzo[1',10']phenanthro[3',4':4,5]thieno[3,2-*b*]benzo[1,10]phenanthro[3,4-*d*]thiophene coupled with a diarylamine electron-donor and 4-(7-ethynylbenzo[*c*][1,2,5]thiadiazol-4-yl)benzoic acid acceptor. Dye R6 displays a brilliant sapphire color in a sensitized TiO_2 mesoporous film with a Co(II/III)tris(bipyridyl)-based redox electrolyte. The R6 based DSC achieves an impressive power conversion efficiency of 12.6% under standard air mass 1.5 global, 100 mW cm^{-2} and shows a remarkable photostability.

Dye-sensitized solar cells (DSCs)[1–5] can powerfully generate electricity at low-cost.[6] The power conversion efficiency (PCE) of DSCs has steadily increased from 7% in 1991 to 14.3% in 2015 under the standard air mass 1.5 global (AM1.5G) conditions.[1,7] Under artificial indoor lights, they have displayed an outstanding PCE over 20%.[8,9] Benefiting from the flexibility in tailoring dye molecules, especially donor-acceptor photosensitizers, DSCs have a unique property of offering a palette of colors, which is attractive for various applications such as building-integrated photovoltaic (BIPV) windows.[10–13] In 2014, the west façade of the Swiss Tech Convention Center was equipped with the world's first solar window (Figure S1) composed of 1,400 DSC modules (~200 m^2 photoactive area, estimated ~2000 kW h of annual solar electricity generation).[10] Those modules contain five different colors except blue. Such an impressive achievement motivated us to develop efficient, stable blue dye molecules. Although some blue dyes were reported[14–18] and the best PCE was 10.1% achieved by Grätzel and co-workers,[14] their performance and high cost impede practical applications.

Anthracene-based conjugated materials have been developed successfully for blue emitting organic light-emitting diodes,[19–21] thin film transistors,[22] and bulk heterojunction solar cells.[23] However, photosensitizers with anthracene as the kernel segment in DSCs merely displayed a moderate PCE.[9,24–28] Recently, Wang and co-workers reported an organic dye R2 with a polycyclic aromatic hydrocarbon (PAH) core 2*H*-dinaphthopentacene achieving a PCE up to 10.2%.[28]. However, R2 exhibited a narrow spectral response and a modest short-circuit photocurrent density (J_{sc}) of 14.00 mA cm^{-2}.

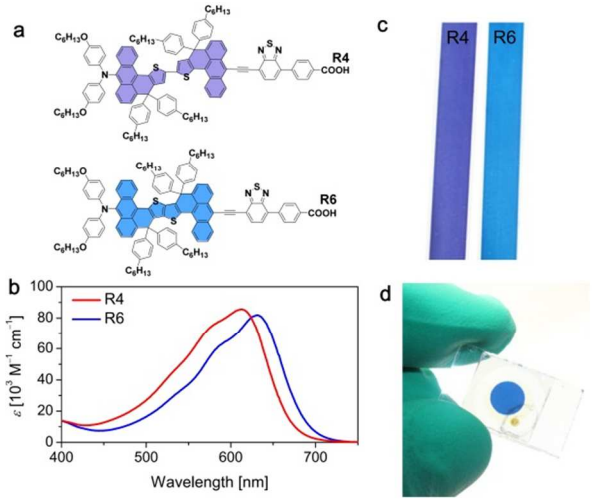

Figure 1. Color palette of photosensitizers achieved by molecular tailoring. (a) Chemical structures of R4 and R6 dye molecules. (b) Spectra of dye molecules in tetrahydrofuran (10 μM). (c) The image of dye-sensitized TiO_2 films (size: 8.5 cm × 1.3 cm). (d) The image of a DSC based on the R6-sensitized nanocrystalline TiO_2 film with a Co(II/III)tris(bipyridyl)-based electrolyte.

Herein, we report a narrow energy-gap, blue dye R6 (Figure 1a) featuring a stronger electron-donating PAH, 9,19-dihydrobenzo[1',10']phenanthro[3',4':4,5]thieno[3,2-*b*]benzo[1,10]phenanthro[3,4-*d*]thiophene (BPT2), compared with 4*H*,4'*H*-2,2'-bibenzo[1,10]phenanthro[4,3-*b*]thiophene (2BPT) in a counterpart dye R4. BPT2 and 2BPT are tethered with an auxil-

iary diarylamine electron-donor and an electron acceptor of 4-(7-ethynylbenzo[*c*][1,2,5]thiadiazol-4-yl)benzoic acid (EBTBA). R6 exhibits a brilliant sapphire color when adsorbed on the TiO_2 film in the presence of a Co(II/III)tris(bipyridyl)-based redox electrolyte. The DSC with R6 achieves an impressive PCE of 12.6% under the standard AM1.5G sunlight and remarkable photostability.

Synthesis of R4 and R6. As illustrated in Scheme S1, we started the synthesis of R6 from the easily available diethyl 2,5-dichlorothieno[3,2-b]thiophene-3,6-dicarboxylate (2).[29] First, compound diethyl 2,5-di(anthracen-9-yl)thieno[3,2-*b*]thiophene-3,6-dicarboxylate (3) was prepared by two-fold Suzuki coupling at 84% yield from 2. Subsequent double Grignard nucleophilic addition of 3 with (4-hexylphenyl)magnesium bromide[30] generated a bis-tertiary alcohol intermediate in square brackets, which was further subjected to an acid-catalyzed intramolecular Friedel-Crafts cyclization to afford the key product 9,9,19,19-tetrakis(4-hexylphenyl)-9,19-dihydrobenzo[1',10']phenanthro[3',4':4,5]thieno[3,2-*b*]benzo[1,10]phenanthro[3,4-*d*]thiophene (4) at 83% yield. Afterwards, the electron-donor *N*,*N*-bis(4-(hexyloxy)phenyl)-9,9,19,19-tetrakis(4-hexylphenyl)-9,19-dihydrobenzo - [1',10']phenanthro[3',4':4,5]thieno[3,2-*b*]benzo[1,10]phenanthro[3,4-d]thiophen-5-amine (6) was obtained at 62% yield via the Buchwald-Hartwig coupling of bis(4-(hexyloxy)phenyl)amine (5)[31] with a bromide gained by the bromination of 4 at room temperature. We further performed monobromination of 6 to obtain a bromide, which was further coupled with butyl 4-(7-ethynylbenzo[*c*][1,2,5]thiadiazol-4-yl)benzoate[32] using the Sonogashira–Hagihara reaction to afford an esterified dye precursor at 86% yield. Eventually, the desired dye R6 was obtained via hydrolysis and acidification at 98% yield over two steps. Following a similar synthetic strategy, dye R4 was obtained from diethyl 5,5'-dibromo-[2,2'-bithiophene]-4,4'-dicarboxylate (10),[33] as shown in Scheme S2.

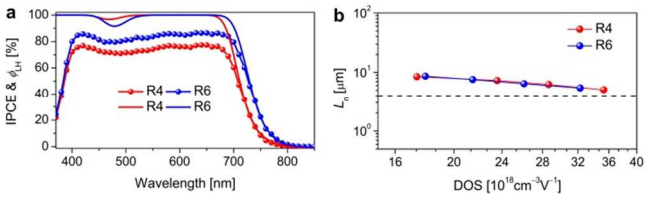

Figure 2. Photocurrent action spectra and charge transport of solar cells. (a) IPCE (dot line) of DSCs and ϕ_{LH} (solid line) of a dye-sensitized TiO_2 film (8.0-μm-thick transparent TiO_2 layer). (b) L_n as a function of *DOS* of DSCs. The dotted line represents the thickness of nanocrystalline TiO_2 layer in the DSCs.

Spectroscopic and electronic properties. Figure 1b shows the wavelength-dependent molar extinction coefficients (ε) of R4 and R6 dissolved in tetrahydrofuran (THF). Both dyes have a strong light-harvesting capability in the red region and a weak absorption in the blue part of the visible spectrum. Their maximum ε are 81.8×10^3 M^{-1} cm^{-1} at 631 nm for R6 and 85.5×10^3 M^{-1} cm^{-1} at 613 nm for R4. Figure 1c shows an image of dye-sensitized TiO_2 films (30 nm sized nanocrystals, 4 μm thick). The R6-sensitized panel displays a shiny blue tint compared with R4-sensitized one. A cell fabricated with 4 μm thick R6-sensitized film in conjunction with a Co(II/III)tris(bipyridyl)-based redox electrolyte also displays attractive sapphire (Figure 1d), enriching the family of colorful DSCs modules. The image of a DSC with R4 was shown in Figure S2.

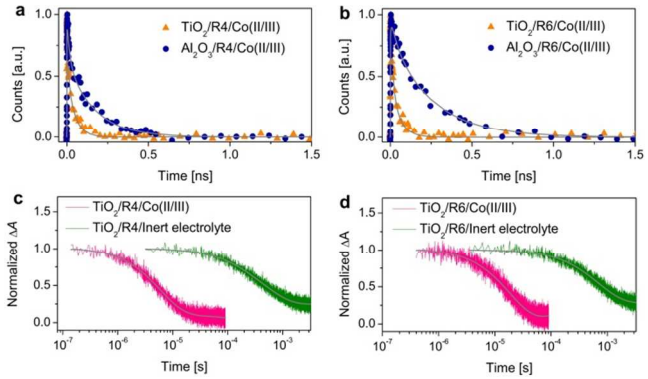

Figure 3. Photo-induced charge transfer of sensitizers. Up-converted PL traces of R4 (a) and R6 (b) grafted mesoporous Al_2O_3 and TiO_2 films. The grey lines are multiexponential fittings. Probe wavelength: 970 nm; pump wavelength: 490 nm; pulse fluence: 28 μJ cm^{-2}. Transient absorption spectra of R4 (c) and R6 (d) grafted TiO_2 films with an inert electrolyte and a Co(II/III)tris(bipyridyl)-based redox electrolyte. The inert electrolyte contains 0.1 M LiTFSI and 0.1 M TBP in acetonitrile. The grey lines are multiexponential fittings. Pump wavelength: 680 nm for R4 and 692 nm for R6; probe wavelength: 850 nm.

To unveil the influences of conjugated-backbone (2BPT vs BPT2) on the highest occupied molecular orbital (HOMO) and lowest unoccupied molecular orbital (LUMO) of R4 and R6, we measured their cyclic voltammograms (CV). Their vacuum energy levels were estimated via the equation $E=-4.88-\mathrm{e}E_{onset}$, where E_{onset} is the onset potential of reduction and oxidation of the ground-state molecule.[34] Figure S3 shows that the alternation of conjugated-backbones hardly affects the HOMO and LUMO energy levels of R4 and R6, both with the HOMO energy level being –4.90 eV and the LUMO being –3.35 eV. The LUMO/HOMO energy gap ($\Delta E_{L/H}^{CV}$) is 1.55 eV. This is in consistent with the results of Density functional theory (DFT) calculations (Figure S4). However, R6 red shifts the maximum absorption by 18 nm and has a lower maximum ε compared to R4 (Figure 1b). This result motivated us to explore their electronic transitions in detail.

In general, the $S_1 \leftarrow S_0$ vertical electronic transitions to LUMO for these two dyes mainly stem from HOMO, displaying a feature of intramolecular charge transfer as perceived from the contour plots of molecular orbitals (Figure S5). The superficial inconsistence between LUMO/HOMO energy gap ($\Delta E_{L/H}^{B3LYP}$, Figure S4) and maximum absorption wavelength calculated at the TD-MPW1K/6-311G(d,p) level of theory ($\lambda_{ABS,MAX}^{TD\text{-}MPW1K}$, Table S1) for R4 and R6 can be better assessed by resorting to the detailed transition assignments tabulated in Table S2. The proportion of excitation from HOMO to LUMO is 80% in R6, compared to 71% in R4. Thus, it is reasonable to detect the red-shifted absorption maxima for R6. Figure S8 shows that the lifetimes of R4 and R6 in THF at the equilibrium excited state are respective 231 and 289 ps (see detailed discussions in Figure S8). This result renders a clue for the judicious design of organic photosensitizers with a rigid PAH.

Photocurrent action spectra and charge transport of solar cells. The monochromatic incident photon-to-electron conversion efficiencies (IPCEs) of DSCs employing R4 or R6 with the Co(II/III)tris(bipyridyl)-based redox electrolyte are displayed in

Figure 2a. The fabrication of devices is elaborated in the Supporting Information. Note that the efficient DSC employs the TiO_2 film composed of a nanocrystalline layer (30 nm sized nanocrystals, 4 μm thick) and a light scattering layer (350-450 nm sized crystals, 5 μm thick). The IPCE of the R6 cell achieves a maximum value of 85%, which is remarkably higher than that of R4 (75%). Additionally, its onset wavelength red shifts by 20 nm compared with that of R4. This result is in accord with the wavelength dependent light-harvesting yields (ϕ_{LH}) (Figure 2a).

Apart from the yield of light harvesting, the yields of charge generation and collection also determine the value of IPCE. Electrical impedance measurements (EIS) show that the electron diffusion length (L_n) as a function of density of states (*DOS*) in DSCs of R4 and R6 are comparable (Figure 2b), indicating that both cells have comparable charge collection yields. Significantly, the L_n in both cells is larger than the thickness of the transparent TiO_2 layer, suggesting close to quantitative charge collection yield.

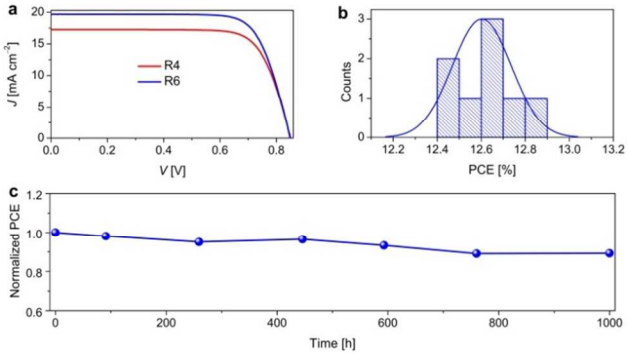

Figure 4. Efficient and photostable blue dye-sensitized solar cells. (a) $J-V$ curves of R4 and R6 based DSCs measured under the 100 mW cm^{-2}, AM1.5G sunlight. (b) Histogram of PCE of DSCs with R6 (eight samples). The Gaussian fit has been added to aid the eye. (c) Normalized PCE of R6 cell measured under the 53.5 mW cm^{-2}, AM1.5 sunlight during the continuous full sunlight soaking at 60 °C for 1,000 h.

Photo-induced charge transfer of sensitizers. We further estimated the yields of electron injection (ϕ_{ei}) from excited-state dye molecules to TiO_2 with femtosecond fluorescence up-conversion measurements.[35–36] First, a control cell based on a dye-grafted mesoporous Al_2O_3 film in the Co(II/III)tris(bipyridyl)-based electrolyte was excited at 490 nm by the femtosecond pulse. The photoluminescence (PL) decays due to radiative and nonradiative deactivation of excited-state dye molecules (blue dots in Figure 3a, 3b) provide amplitude-averaged lifetimes $\overline{\tau}(A)$ of 117 and 260 ps for R4 and R6, respectively. The longer PL lifetime of R6 may stem from its more rigid electronic skeleton. The $\overline{\tau}(T)$ is significantly shortened in working cells where the dyes are adsorbed on mesoporous TiO_2 films, both being 26 ps. Note that $\overline{\tau}(A)$ and $\overline{\tau}(T)$ herein are the equilibrium excited state lifetimes (see detailed discussions in Figure S13). The ϕ_{ei} can be estimated from the equation $\phi_{ei} = 1-\overline{\tau}(T)/\overline{\tau}(A)$, being 78% for R4 and 88% for R6. The higher ϕ_{ei} for R6 can be understood by its longer equilibrium excited state lifetime on Al_2O_3. This result gives a distinct clue for the relative difference in the IPCE values.

We further used the nanosecond laser flash photolysis spectrometer to monitor the kinetics of dual-path charge-transfer reactions of photooxidized dye molecules (D^+) either with free electrons in TiO_2 or with cobalt(II) ions in the electrolyte. The absorption traces can be well fitted with multiexponential functions for convenient determination of half-reaction times ($\tau_{1/2}$). For the dye-sensitized TiO_2 films with an inert electrolyte (0.1 M lithium bis(trifluoromethanesulfonyl)imide (LiTFSI) and 0.1 M 4-*tert*-butylpyridine (TBP) in acetonitrile), the decay signals (Figure 3c, 3d) are related to the back electron transfer from TiO_2 to D^+. The $\tau_{1/2}$ for this process are 0.48 ms for R4 and 0.84 ms for R6. For the films with the Co(II/III)tris(bipyridyl)-based electrolyte, accelerated decay signals imply the occurrence of hole injection from D^+ to cobalt (II) ions, the $\tau_{1/2}$ of which are 5.0 μs for R4 and 14.6 μs for R6. Overall, the hole injection yields (ϕ_{hi} , $\phi_{hi}=1-\tau_{1/2}^{Co\text{-}bpy}/\tau_{1/2}^{inert}$) for R4 and R6 are 99% and 98%, respectively.

Table 1. Photovoltaic Parameters Measured under the AM1.5G Sunlight

Dye	J_{SC}^{EQE} [mA cm^{-2}]	J_{SC} [mA cm^{-2}]	V_{OC} [mV]	FF [%]	PCE [%]
R4	16.80±0.04	17.25±0.2	852±3	75.4±0.1	11.1±0.1
R6	19.36±0.04	19.69±0.15	850±3	75.4±0.2	12.6±0.2

Efficient and photostable blue dye-sensitized solar cells. The photocurrent density–voltage ($J-V$) curves (Figure 4a) of DSCs with R4 and R6 were measured under the standard AM1.5G, 100 mW cm^{-2} conditions. The averaged parameters of eight cells made with each dye are compiled in Table 1. The R4 cell delivers a J_{SC} of 17.25 mA cm^{-2}, an open-circuit photovoltage (V_{OC}) of 852 mV, and a fill factor (FF) of 75.4%, yielding a PCE of 11.1%. Impressively, the R6 cell has the PCE of 12.6%, produced from the J_{SC} of 19.69 mA cm^{-2}, the V_{OC} of 850 mV, and the FF of 75.4%. The comparable V_{OC} of both cells is due to their similar electron lifetimes (Figure S15a) and profiles of charges (Q^{CE}) stored in TiO_2 (Figure S15b). The higher J_{SC} of R6 than that of R4 benefits from the wider spectrum response and the higher IPCE peak value. The integrals of IPCE (19.36 mA cm^{-2}) over the standard AM1.5G emission spectrum (ASTM G173-03) is in agreement with the obtained photocurrent density (J_{SC} = 19.69 mA cm^{-2}). The PCE histogram of the R6 cell is presented in Figure 4b. The normalized PCE of R6 measured at an irradiance of 53.5 mW cm^{-2} maintains 90% of its initial value after 1,000 h of continuous full sunlight soaking at 60 °C (Figure 4c). The detailed photovoltaic parameters are presented in Figure S16. Together with champion green (11.9%)[37] and red dyes (14.3%),[7] R6 is the best candidate so far in the family of blue dyes for the color palette of DSCs.

In summary, we report a novel blue dye R6 characteristic of electron-rich PAH of 2*H*-benzophenanthrothienobenzophenanthrothiophene. R6 sensitized TiO_2 film displays attractive blue sapphire color, filling the color gap of DSCs modules. The DSC with R6 achieves an impressive PCE of 12.6% under the full sunlight, which is so far the best performance in the family of blue dyes for DSCs. The R6 cell also displays a remarkable photostability, promising the color palette of DSCs to be applied in sunroofs and BIPV.

ASSOCIATED CONTENT

Supporting Information

The Supporting Information is available free of charge on the ACS Publications website at DOI:
Details of the synthesis and characterization of the dyes, theoretical calculations, electrochemical and photophysical measurements (CV, EIS, nanosecond laser flash photolysis, femtosecond fluorescence up-conversion, transient photovoltage decay, and charge extraction), and cell fabrication (PDF)

AUTHOR INFORMATION

Corresponding Author

* pw2015@zju.edu.cn
*michael.graetzel@epfl.ch

Notes

The authors declare no competing financial interests.

ACKNOWLEDGMENT

P.W. acknowledges financial support from the National Science Foundation of China (No. 51673165 and 91233206), the National 973 Program (2015CB932204), and the Key Technology R&D Program (BE2014147-1) of Science and Technology Department of Jiangsu Province. M.G. acknowledges financial support from Swiss National Science Foundation, CTI 17622.1 PFNM-NM, and g2e.

REFERENCES

1. O'Regan, B.; Grätzel, M. *Nature* **1991**, *353*, 737.
2. Bach, U.; Lupo, D.; Comte, P.; Moser, J. E.; Weissörtel, F.; Salbeck, J.; Spreitzer, H.; Grätzel, M. *Nature*, **1998**, *395*, 583.
3. Grätzel, M. *Nature*, **2001**, *414*, 338.
4. Grätzel, M.; Janssen, R. A. J.; Mitzi, D. B.; Sargent, E. H. *Nature* **2012**, *488*, 304.
5. Mathew, S.; Yella, A.; Gao, P.; Humphry-Baker, R.; Curchod, B. F. E.; Ashari-Astani, N.; Tavernelli, I.; Rothlisberger, U.; Nazeeruddin, M. K.; Grätzel, M. *Nat. Chem.* **2014**, *6*, 242.
6. Kawakita J. *Sci. Technol. Trends* **2010**, *35*, 70.
7. Kakiage, K.; Aoyama, Y.; Yano, T.; Oya, K.; Fujisawa, J.-i.; Hanaya, M. *Chem. Commun.* **2015**, *51*, 15894.
8. Freitag, M.; Teuscher, J.; Saygili, Y.; Zhang, X.; Giordano, F.; Liska, P.; Hua, J.; Zakeeruddin, S. M.; Moser, J.-E.; Grätzel, M.; Hagfeldt, A. *Nat. Photonics* **2017**, *11*, 372.
9. Tingare, Y. S.; Vinh, N. S.; Chou, H.-H.; Liu, Y.-C.; Long, Y.-S.; Wu, T.-C.; Wei, T.-C.; Yeh, C.-Y. *Adv. Energy Mater.* **2017**, *7*, 1700032.
10. Fakharuddin, A.; Jose, R.; Brown, T. M.; Fabregat-Santiago, F.; Bisquert, J. *Energy Environ. Sci.* **2014**, *7*, 3952.
11. Yoon, S.; Tak, S.; Kim, J.; Jun, Y.; Kang, K.; Park, J. *Building and Environment*, **2011**, *46*, 1899.
12. Heiniger, L.-P.; O'Brien, P. G.; Soheilnia, N.; Yang, Y.; Kherani. N. P.; Grätzel, M.; Ozin, G. A.; Tétreault, N. *Adv. Mater.* **2013**, *25*, 5734.
13. Zhang, K.; Qin, C.; Yang, X.; Islam, A.; Zhang, S.; Chen, H.; Han, L. *Adv. Energy Mater.* **2014**, *4*, 1301966.
14. Yum, J.-H.; Holcombe, T. W.; Kim, Y.; Rakstys, K.; Moehl, T.; Teuscher, J.; Delcamp, J. H.; Nazeeruddin, M. K.; Grätzel, M. *Sci. Rep.* **2013**, *3*, 2446.
15. Mao, J.; Yang, J.; Teuscher, J.; Moehl, T.; Yi, C.; Humphry-Baker, R.; Comte, P.; Grätzel, C.; Hua, J.; Zakeeruddin, S. M.; Tian, H.; Grätzel, M. *J. Phys. Chem. C* **2014**, *118*, 17090.
16. Zhang, J.; Vlachopoulos, N.; Hao, Y.; Holcombe, T. W.; Boschloo, G.; Johansson, E. M. J.; Grätzel M.; Hagfeldt, A. *ChemPhysChem* **2016**, *17*, 1441.
17. Hao, Y.; Saygili, Y.; Cong, J.; Eriksson, A.; Yang, W.; Zhang, J.; Polanski, E.; Nonomura, K.; Zakeeruddin, S. M.; Grätzel M.; Hagfeldt, A.; Boschloo, G. *ACS Appl. Mater. Interfaces* **2016**, *8*, 32797.
18. Shen, Z.; Xu, B.; Liu, P.; Hu, Y.; Ding, H.; Kloo, L.; Hua, J.; Sun, L.; Tian, H. *J. Mater. Chem. A* **2017**, *5*, 1242.
19. Shi, J.; Tang, C. W. *Appl. Phys. Lett.* **2002**, *80*, 3201.
20. Lee, M.-T.; Liao, C.-H.; Tsai, C.-H.; Chen. C. H. *Adv. Mater.* **2005**, *17*, 2493.
21. Reddy, M. A.; Thomas, A.; Srinivas, K.; Rao, V. J.; Bhanuprakash, K.; Sridhar, B.; Kumar, A.; Kamalasanan, M. N.; Srivastava, R. *J. Mater. Chem.* **2009**, *19*, 6172.
22. Silvestri, F.; Marrocchi, A.; Seri, M.; Kim, C.; Mark, T. J.; Facchetti, A.; Taticchi, A. *J. Am. Chem. Soc.* **2010**, *132*, 6108.
23. Valentini, L.; Bagnis, D.; Marrocchi, A.; Seri, M.; Taticchi, A.; Kenny, J. M. *Chem. Mater.* **2008**, *20*, 32.
24. Srinivas, K.; Yesudas, K.; Bhanuprakash, K.; Rao, V. J.; Giribabu, L. *J. Phys. Chem. C* **2009**, *113*, 20117.
25. Bouit, P.-A.; Marszalek, M.; Hummphry-Baker, R.; Viruela, R.; Ortí, E.; Zakeeruddin, S. M.; Grätzel, M.; Delgado, J. L.; Martín, N. *Chem.–Eur. J.* **2012**, *18*, 11621.
26. Lin, R. Y.; Lin, H. W.; Yen, Y. S.; Chang, C. H.; Chou, H. H.; Chen, P .W.; Hsu, C. Y.; Chen, Y. C.; Lin, J. T.; Ho, K. C. *Energy Environ. Sci.* **2013**, *6*, 2477.
27. Lin, Y. Z.; Huang, C. H.; Chang, Y. J.; Yeh, C. W.; Chin, T. M.; Chi, K. M.; Chou, P. T.; Watanabe, M.; Chow, T. J. *Tetrahedron* **2014**, *70*, 262.
28. Ren Y.; Liu, J.; Zheng, A.; Dong, X.; Wang, P. *Adv. Sci.* **2017**, 1700099.
29. Kunz, T.; Knochel, P. *Chem. Eur. J.* **2011**, *17*, 866.
30. Cai, N.; Li, R.; Wang, Y.; Zhang, M.; Wang, P. *Energy Environ. Sci*. **2013**, *6*, 139.
31. Yao, Z.; Yan, C.; Zhang, M.; Li, R.; Cai, Y.; Wang, P. *Adv. Energy Mater.* **2014**, *4*, 1400244.
32. Yang, L.; Ren, Y.; Yao, Z.; Yan, C.; Ma, W.; Wang, P. *J. Phys. Chem. C* **2015**, *119*, 980.
33. Sakamoto, K.; Takashima, Y.; Hamada, N.; Ichida, H.; Yamaguchi, H.; Yamamoto, H.; Harada, A. *Org. Lett.* **2011**, *4*, 672.
34. Cardona, C. M.; Li, W.; Kaifer, A. E.; Stockdale, D.; Bazan, G. C. *Adv. Mater.* **2011**, *23*, 2367.
35. Lin, C. Y.; Lo, C. F.; Luo, L.; Lu, H. P.; Hung, C. S.; Diau, E. W. G. *J. Phys. Chem. C* **2009**, *113*, 755.
36. Fakis, M.; Stathatos, E.; Tsigaridas, G.; Giannetas, V.; Persephonis, P. *J. Phys. Chem. C* **2011**, *115*, 13429.
37. Yella, A.; Lee, H.-W.; Tsao, H. N.; Yi, C.; Chandiran, A. K.; Nazeeruddin, M. K.; Diau, E. W.-G.; Yeh, C.-Y.; Zakeeruddin, S. M.; Grätzel, M. *Science* **2011**, *334*, 629.

TOC